

## Atomic layer deposited aluminium phosphate thin films on N-doped CNTs†

Cite this: *RSC Advances*, 2013, 3, 4492

Received 14th December 2012,

Accepted 24th January 2013

DOI: 10.1039/c3ra23320k

[www.rsc.org/advances](http://www.rsc.org/advances)

Jian Liu,<sup>a</sup> Yongji Tang,<sup>ab</sup> Biwei Xiao,<sup>a</sup> Tsun-Kong Sham,<sup>b</sup> Ruying Li<sup>a</sup> and Xueliang Sun<sup>\*a</sup>

**Uniform amorphous aluminium phosphate thin films with precisely controlled thickness and tunable composition were deposited on nitrogen-doped carbon nanotubes at 150 °C through a new atomic layer deposition approach.**

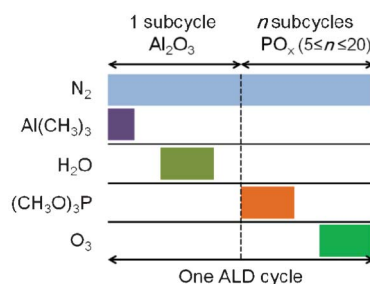
Aluminium phosphate (AlPO<sub>4</sub>) has long been known as a catalyst support for numerous catalytic applications.<sup>1,2</sup> AlPO<sub>4</sub> itself has been used to catalyze the dehydration of methanol to dimethyl ether, which is a clean alternative fuel for diesel engines and a potential aerosol propellant in the cosmetics industry.<sup>3</sup> AlPO<sub>4</sub> coating on cathodes has been considered as an effective strategy to improve both the safety and cycle-performance of lithium secondary batteries.<sup>4</sup> In addition, an AlPO<sub>4</sub> protective layer has been shown to inhibit the oxidation of carbonaceous materials.<sup>5</sup>

AlPO<sub>4</sub> has generally been synthesized previously through a co-precipitation process followed by heat treatment.<sup>1–5</sup> Unfortunately, this route is incapable of achieving uniform aluminium phosphate thin films and lacks the flexibility to tune their chemical composition (P/Al ratio). Uniformity and tunable composition have been proven to play a critical role in determining the practical applications of AlPO<sub>4</sub>.<sup>3,6</sup> Recently, atomic layer deposition (ALD) has emerged as a powerful technique for thin film deposition.<sup>7,8</sup> Unlike other physical or chemical vapour deposition processes, ALD employs alternative precursor doses and self-limiting surface reactions, which result in material growth of one monolayer (or less) per cycle. Thus, ALD offers exquisite control over the thickness and composition of thin films. However, there have been very few studies on the preparation of aluminium phosphate by ALD.<sup>9–11</sup> Aluminium phosphate was found to form in P-doped aluminium oxide with P doping greater than 10 wt% at

450 and 500 °C using AlCl<sub>3</sub> or aluminium *n*-propoxide, 2-methyl-2-propanol and P<sub>2</sub>O<sub>5</sub> as precursors.<sup>10</sup> However, the high deposition temperature seriously hinders its applications, especially for sensitive substrates. In another study, aluminium phosphate was obtained from AlCl<sub>3</sub> and trimethylphosphate at deposition temperatures between 150 and 400 °C.<sup>11</sup> This route simplifies the ALD process by sacrificing the controllability of the chemical composition of the aluminium phosphates. Moreover, the use of metal chlorides is undesirable in the ALD process, because it may lead to the corrosion of the ALD system caused by HCl generated during the reaction and leave Cl impurities in the deposited films.<sup>11,12</sup>

Herein, we report a new ALD approach to fabricate amorphous aluminium phosphate (Al<sub>x</sub>P<sub>y</sub>O<sub>z</sub>) thin films. Its features include low-temperature deposition, controllable film thickness, variable film composition, and freedom from metal chlorides. Al<sub>x</sub>P<sub>y</sub>O<sub>z</sub> thin films are deposited by combining subcycles of Al<sub>2</sub>O<sub>3</sub> and PO<sub>x</sub>, and one ALD cycle consists of 1 Al<sub>2</sub>O<sub>3</sub> subcycle and *n* PO<sub>x</sub> subcycles (5 ≤ *n* ≤ 20) (Scheme 1). The popular trimethylaluminium (TMA)–H<sub>2</sub>O is adopted for the Al<sub>2</sub>O<sub>3</sub> subcycle, and trimethylphosphite (TMP)–O<sub>3</sub> is used for the PO<sub>x</sub> subcycle. The composition (P/Al ratio) of Al<sub>x</sub>P<sub>y</sub>O<sub>z</sub> thin films is controlled by varying the PO<sub>x</sub> subcycles while keeping the Al<sub>2</sub>O<sub>3</sub> subcycle unchanged.

Nitrogen-doped carbon nanotubes (NCNTs) grown on carbon papers are employed as substrates for the deposition of Al<sub>x</sub>P<sub>y</sub>O<sub>z</sub> thin films, due to their defective surface, which is ready for the



**Scheme 1** Illustration of the ALD process for aluminium phosphate.

<sup>a</sup>Department of Mechanical and Materials Engineering, University of Western Ontario, London, ON, Canada N6A 5B9. E-mail: [xsun@eng.uwo.ca](mailto:xsun@eng.uwo.ca); Fax: 1 519 661 3020; Tel: 1 519 661 2111 Ext. 87759

<sup>b</sup>Department of Chemistry, University of Western Ontario, London, ON, Canada, N6A 5B7

† Electronic supplementary information (ESI) available: TEM image of NCNTs; XRD pattern of 100-cycle Al<sub>1.3</sub>PO<sub>5.0</sub>; XPS of Al 2p, P 2p and O 1s peaks for Al<sub>1.3</sub>PO<sub>5.0</sub>; TEM and HRTEM images of NCNTs coated with Al<sub>1.3</sub>PO<sub>5.0</sub> for 25, 50 and 75 ALD cycles; EDS of Al<sub>x</sub>P<sub>y</sub>O<sub>z</sub> deposited using different PO<sub>x</sub> subcycles; HRTEM images of NCNTs coated with 50-cycle thin films using different recipes. See DOI: 10.1039/c3ra23320k

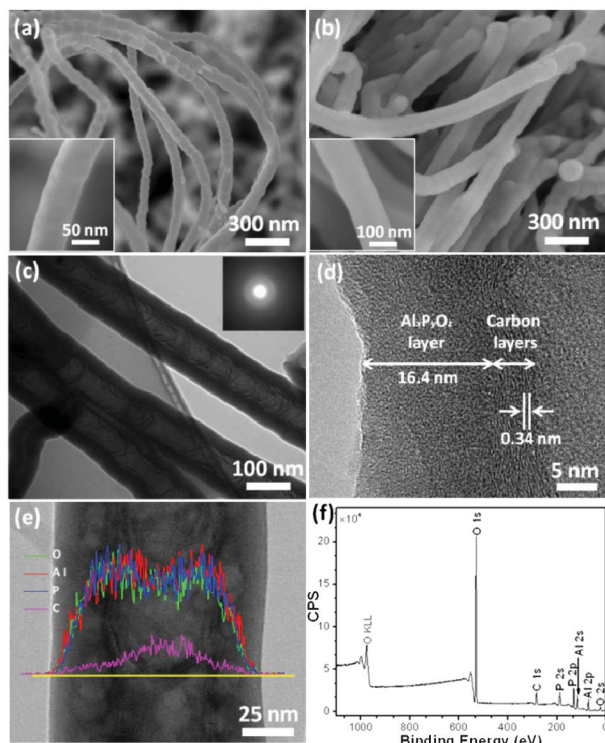


**Fig. 1** (a) SEM image of NCNTs; (b) SEM image, (c) TEM image, (d) HRTEM image, (e) STEM-EDS line-scanning and (f) XPS spectrum of NCNTs coated with 100-cycle  $\text{Al}_x\text{P}_y\text{O}_z$  thin film deposited using a sequence of  $1 \times (\text{TMA}-\text{H}_2\text{O})-20 \times (\text{TMP}-\text{O}_3)$ .

growth of metal oxides.<sup>13,14</sup> The deposition of  $\text{Al}_x\text{P}_y\text{O}_z$  is performed at 150 °C by sequentially introducing TMA,  $\text{H}_2\text{O}$ , TMP and  $\text{O}_3$  (9.8 wt% concentration) into the ALD reaction chamber. The ALD sequence is described as  $1 \times (\text{TMA}-\text{H}_2\text{O})-n \times (\text{TMP}-\text{O}_3)$  ( $n = 5, 10$  and 20). The pulse time is 0.5, 1, 1 and 1 s for TMA,  $\text{H}_2\text{O}$ , TMP and  $\text{O}_3$  respectively, and the purge time after each pulse is 15 s.

The initial NCNTs have diameters of about 60 nm (Fig. 1a) and exhibit a typical bamboo-like structure (Fig. S1†). Fig. 1b shows a scanning electron microscopy (SEM) image of a 100-cycle  $\text{Al}_x\text{P}_y\text{O}_z$  thin film deposited on NCNTs using the sequence of  $1 \times (\text{TMA}-\text{H}_2\text{O})-20 \times (\text{TMP}-\text{O}_3)$ . It is apparent from Fig. 1b and 1c that the coating of the thin film is uniform and conformal on NCNTs, and the diameter of the nanotubes increases to  $\sim 100$  nm. The selected area diffraction (SAD) pattern in Fig. 1c indicates that the 100-cycle  $\text{Al}_x\text{P}_y\text{O}_z$  thin film is amorphous, which is confirmed by the X-ray diffraction pattern (Fig. S2†) and high resolution transmission electron microscopy (HRTEM) image in Fig. 1d. From Fig. 1d, the thickness of the  $\text{Al}_x\text{P}_y\text{O}_z$  thin film is measured to be 16.4 nm. Fig. 1e presents the energy dispersive X-ray spectroscopy (EDS) elemental line-scanning result of the 100-cycle  $\text{Al}_x\text{P}_y\text{O}_z$  thin film from scanning transmission electron microscopy (STEM). Fig. 1e clearly indicates the homogeneous distribution of Al, P and O elements along the carbon nanotube. X-ray photoelectron spectroscopy (XPS) analysis shows that the composition of Al, P and O elements is 15.4, 11.5 and 57.8 at% respectively, as shown in Fig. 1f (the deconvolution of the Al 2p, P

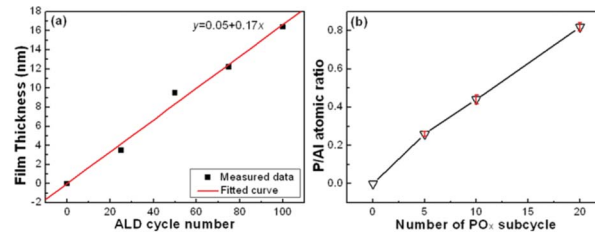


**Fig. 2** (a) Film thickness of  $\text{Al}_{1.3}\text{PO}_{5.0}$  as a function of ALD cycle number and (b) P/Al atomic ratio in  $\text{Al}_x\text{P}_y\text{O}_z$  thin films deposited using  $1 \times (\text{TMA}-\text{H}_2\text{O})-n \times (\text{TMP}-\text{O}_3)$  ( $n = 5, 10$  and 20).

2p and O 1s peaks is provided in Fig. S3†). Thereby, the chemical formula is determined to be  $\text{Al}_{1.3}\text{PO}_{5.0}$  for the aluminium phosphate thin film deposited using an ALD sequence of  $1 \times (\text{TMA}-\text{H}_2\text{O})-20 \times (\text{TMP}-\text{O}_3)$ .

$\text{Al}_{1.3}\text{PO}_{5.0}$  thin films produced with 25, 50 and 75 ALD cycles were also examined, and their uniformity on the NCNTs was observed in TEM and HRTEM images (Fig. S4†). The thickness of the thin film was measured to be 3.5, 9.5 and 12.2 nm for  $\text{Al}_{1.3}\text{PO}_{5.0}$  deposited with 25, 50 and 75 ALD cycles respectively. Film thickness is plotted as a function of ALD cycles in Fig. 2a. The film thickness has a linear relationship with the number of ALD cycles, indicating the self-limiting nature of this ALD process. Growth per cycle for the  $\text{Al}_{1.3}\text{PO}_{5.0}$  thin film at 150 °C was determined to be 1.7 Å per cycle by fitting the data in Fig. 2a linearly. Thus, an aluminium phosphate thin film with a desired thickness can be easily obtained by choosing an appropriate number of ALD cycles. The growth rate of  $\text{Al}_{1.3}\text{PO}_{5.0}$  is slightly higher than that of aluminium phosphate deposited by ALD from  $\text{AlCl}_3$  and trimethylphosphate (1.4 Å per cycle) at the same deposition temperature.<sup>11</sup>

To demonstrate the flexibility to modify the composition of  $\text{Al}_x\text{P}_y\text{O}_z$  through this ALD approach, we varied the number of  $\text{PO}_x$  subcycles from 20 to 10 and 5, while the  $\text{Al}_2\text{O}_3$  subcycle was kept unchanged. The average P/Al atomic ratio of each sample was obtained from 10 EDS results (Fig. S5†), and is plotted as a function of the number of  $\text{PO}_x$  subcycles in Fig. 2b. One can see that the P/Al atomic ratio decreases from  $\sim 0.8$  to 0.4 to 0.3, when the number of  $\text{PO}_x$  subcycles is reduced from 20 to 10 to 5 respectively. It is worth noting that the P/Al ratio in  $\text{Al}_x\text{P}_y\text{O}_z$  thin films could be adjusted to be either higher or lower by changing the number of  $\text{PO}_x$  subcycles in this ALD recipe. It also should be mentioned that the growth rate of  $\text{Al}_x\text{P}_y\text{O}_z$  thin films would be reduced by lowering the P/Al atomic ratio or the number of  $\text{PO}_x$  subcycles (Fig. S6†), due to the lower contribution of the  $\text{PO}_x$  subcycles to the thin film.

The structure of the amorphous  $\text{Al}_{1.3}\text{PO}_{5.0}$  thin film was analyzed by X-ray absorption near-edge structure (XANES) spectroscopy. Fig. 3 displays the XANES spectra at the Al  $L_{3,2}$ -edge and P  $L_{3,2}$ -edge for  $\text{Al}_{1.3}\text{PO}_{5.0}$ , in comparison with those of standard crystalline  $\text{AlPO}_4$ ,  $\text{Al}_2\text{O}_3$  and  $\text{P}_2\text{O}_5$ . Fig. 3a indicates that  $\text{Al}_{1.3}\text{PO}_{5.0}$  has a very similar Al  $L_{3,2}$ -edge spectrum to standard  $\text{AlPO}_4$ , except that the first transition of  $\text{Al}_{1.3}\text{PO}_{5.0}$  exhibits only one broad peak at 78.3 eV, instead of two well resolved peaks at 77.9 and 78.3 eV

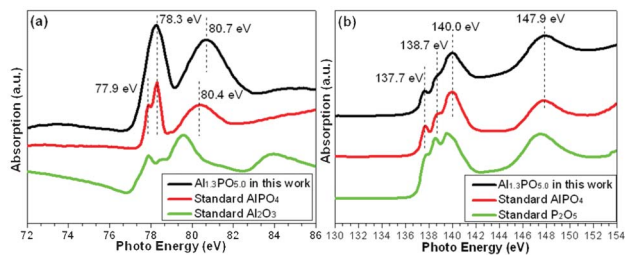


**Fig. 3** XANES Al  $L_{3,2}$ -edge (a) and P  $L_{3,2}$ -edge (b) spectra of  $Al_{1.3}PO_{5.0}$  in this work, and standard  $AlPO_4$ ,  $Al_2O_3$  and  $P_2O_5$ .

for standard  $AlPO_4$ . This observation is attributable to the amorphous state of  $Al_{1.3}PO_{5.0}$ .<sup>15</sup> The first transition in  $Al_{1.3}PO_{5.0}$  could be assigned to transitions from the Al spin-orbit split 2p orbitals to the unoccupied densities of states of 3s character ( $L_3$  and  $L_2$  edges), and the second transition corresponds to transitions from the Al 2p orbitals to the upper bands and is sometimes referred to as a multiple scattering resonance of which the energy position relative to the threshold is related to the inter-atomic distance ( $r$ ) between Al and its nearest neighbouring O atom with a  $\sim 1/r^2$  correlation.<sup>16</sup> A small shift in this resonance to a higher energy indicates that the Al–O inter-atomic distance is shorter in  $Al_{1.3}PO_{5.0}$  compared to  $AlPO_4$  albeit very slightly. It should be noted that the Al  $L_{3,2}$ -edge spectrum of  $Al_{1.3}PO_{5.0}$  distinctly differs from that of  $Al_2O_3$ , owing to the different local bonding environments of the Al sites, *i.e.* P–O–Al in  $Al_{1.3}PO_{5.0}$  and Al–O–Al in  $Al_2O_3$ .<sup>15</sup> In Fig. 3b,  $Al_{1.3}PO_{5.0}$  and standard  $AlPO_4$  exhibit the same four peaks centred at 137.7, 138.7, 140.0 and 147.9 eV in the P  $L_{3,2}$ -edge XANES spectrum, suggesting the same coordination of P (P–O–Al) in both samples and that the local structure of the  $PO_4$  moiety remains intact. The result is in agreement with the P  $L_{3,2}$ -edge XANES spectrum reported for  $AlPO_4$  in the literature.<sup>17</sup> The P  $L_{3,2}$ -edge XANES spectrum of  $Al_{1.3}PO_{5.0}$  is apparently different from that of  $P_2O_5$  (P–O–P). The XANES results provide strong evidence of P–O–Al bonds existing in the amorphous  $Al_{1.3}PO_{5.0}$  thin film prepared by ALD.

The oxidation resistance of carbonaceous materials (carbon fibres, graphite *etc.*) needs to be improved in order to reach the full potential of carbon/carbon composites for high-temperature applications.<sup>18,19</sup> Coating protective layers on carbon materials has been considered as an effective strategy for this purpose.<sup>19</sup> The retarding effect of  $Al_{1.3}PO_{5.0}$  on carbon oxidation has been demonstrated on powder-based NCNTs.<sup>20</sup> Fig. 4 presents differential scanning calorimetry (DSC) and thermogravimetric (TG) curves of NCNTs and NCNTs coated with a 50-cycle  $Al_{1.3}PO_{5.0}$  thin film by ALD (around 10 nm in thickness). The DSC results in Fig. 4a show that the exothermic peak for carbon oxidation shifts from about 480 °C for NCNTs to 550 °C for  $Al_{1.3}PO_{5.0}/NCNTs$ , proving the improved thermal stability of NCNTs by an  $Al_{1.3}PO_{5.0}$  coating. It should be noted that the oxidation temperature of NCNTs in this work ( $\sim 480$  °C) is much lower than that of carbon nanotubes reported previously ( $\sim 650$  °C) because of the N doping.<sup>21</sup> An exothermic shoulder observed at  $\sim 460$  °C in  $Al_{1.3}PO_{5.0}/NCNTs$  is attributed to the transition from amorphous

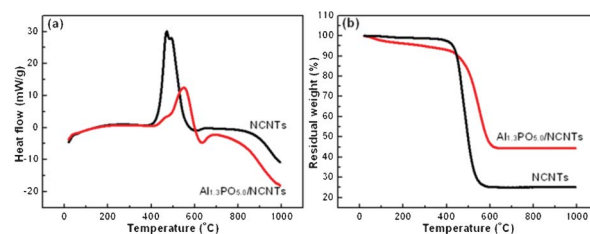


**Fig. 4** DSC (a) and TG (b) curves of NCNTs and 50-cycle  $Al_{1.3}PO_{5.0}$  coated NCNTs conducted at a temperature increase rate of  $10$  °C  $min^{-1}$  in a flowing air atmosphere.

to crystalline  $AlPO_4$ .<sup>22</sup> The TG results in Fig. 4b also suggest the delayed oxidation of NCNTs is caused by the  $Al_{1.3}PO_{5.0}$  coating. For  $Al_{1.3}PO_{5.0}/NCNTs$ , gradual and slow weight loss is found before 440 °C, and could be ascribed to the removal of adsorbed and/or coordinated water.<sup>22,23</sup>  $Al_{1.3}PO_{5.0}$  accounts for 20 wt% of the total weight of  $Al_{1.3}PO_{5.0}/NCNTs$ . From the above results, it can be found that  $Al_{1.3}PO_{5.0}$  thin film made by ALD is an effective protective layer for delaying the oxidation of NCNTs, and its function is comparable to other protective layers, such as zirconia, alumina and/or titania and  $SiC_xO_y$ .<sup>18,21,24</sup> Taking the advantages of uniform, conformal and thickness-controlled film deposition, it is expected that ALD will play an important role in improving the oxidation resistance of carbonaceous materials in the near future.

In conclusion, we report a new low-temperature ALD process to synthesize aluminium phosphate thin films on NCNTs in a well-controlled manner. The film thickness of aluminium phosphates is tunable at the nanoscale level by simply varying the number of ALD cycles, and the film composition (P/Al ratio) is tailored by changing the subcycle ratio between  $Al_2O_3$  and  $PO_x$  during the ALD process. Moreover, the aluminium phosphate film exhibits an inhibitory effect on the oxidation of NCNTs. The strategy reported in this work is applicable to the development of other metal phosphates ( $FePO_4$ ,  $TiPO_4$ ) and phosphate-containing compounds (NASICON-type all-solid-state electrolytes,  $LiM_2(PO_4)_3$  ( $M = Ti, Zr, Ge$  and  $Hf$ )), which will be key components in the next-generation of microbatteries.<sup>25</sup>

## Acknowledgements

The authors acknowledge the support of the Natural Sciences and Engineering Research Council of Canada (NSERC), the Canada Research Chair (CRC) Program, the Foundation for Innovation (CFI), the Ontario Research Fund (ORF), the Canadian Light Source (CLS) at the University of Saskatchewan, and the University of Western Ontario.

## Notes and references

- 1 T. T. P. Cheung, K. W. Willcox, M. P. McDaniel and M. M. Johnson, *J. Catal.*, 1986, **102**, 10.
- 2 M. A. Aramendia, V. Borau, C. Jiménez, J. M. Marinas and J. A. Pajares, *J. Catal.*, 1982, **78**, 188.
- 3 F. Yaripour, M. Mollavali, Sh. M. Jam and H. Atashi, *Energy Fuels*, 2009, **23**, 1896.

- 4 J. Cho, Y-W. Kim, B. Kim, J-G. Lee and B. Park, *Angew. Chem., Int. Ed.*, 2003, **42**, 1618.
- 5 C. R. Maier and L. E. Jones, *Carbon*, 2005, **43**, 2272.
- 6 V. S. Kumar, A. H. Padmasri, C. V. V. Satyanarayana, I. A. K. Reddy, B. D. Raju and K. S. R. Rao, *Catal. Commun.*, 2006, **7**, 745.
- 7 S. M. George, *Chem. Rev.*, 2010, **110**, 111.
- 8 R. L. Puurunen, *J. Appl. Phys.*, 2005, **97**, 121301.
- 9 M. Nieminen, L. Niinistö and R. Lappalainen, *Microchim. Acta*, 1995, **119**, 13.
- 10 M. Tiita, E. Nykänen, P. Soininen, L. Niinistö, M. Leskelä and R. Lappalainen, *Mater. Res. Bull.*, 1998, **33**, 1315.
- 11 J. Hämäläinen, J. Holopainen, F. Munnik, M. Heikkilä, M. Ritala and M. Leskelä, *J. Phys. Chem. C*, 2012, **116**, 5920.
- 12 W-H. Nam and S-W. Rhee, *Chem. Vap. Deposition*, 2004, **10**, 201.
- 13 X. Meng, Y. Zhong, Y. Sun, M. N. Banis, R. Li and X. Sun, *Carbon*, 2011, **49**, 1133.
- 14 J. Liu, X. Meng, M. N. Banis, M. Cai, R. Li and X. Sun, *J. Phys. Chem. C*, 2012, **116**, 14656.
- 15 Y. F. Hu, R. K. Xu, J. J. Dynes, R. I. R. Blyth, G. Yu, L. M. Kozak and P. M. Huang, *Geochim. Cosmochim. Acta*, 2008, **72**, 1959.
- 16 M. Kasrai, M. E. Fleet, T. K. Sham and G. M. Bancroft, *Solid State Commun.*, 1988, **68**, 507.
- 17 J. Kruse, P. Leinweber, K-U. Eckhardt, F. Godlinski, Y. Hu and L. Zuin, *J. Synchrotron Radiat.*, 2009, **16**, 247.
- 18 A. K. Roy, S. Schulze, M. Hietschold and W. A. Goedel, *Carbon*, 2012, **50**, 761.
- 19 C. R. Maier and L. E. Jones, *Carbon*, 2005, **43**, 2272.
- 20 J. Liu, Y. Zhang, M. I. Ionescu, R. Li and X. Sun, *Appl. Surf. Sci.*, 2011, **257**, 7837.
- 21 M. Luo, Y. Li, S. Jin, S. Sang and L. Zhao, *Ceram. Int.*, 2011, **37**, 3055.
- 22 B. Boonchom and S. Kongtaweelert, *J. Therm. Anal. Calorim.*, 2010, **99**, 531.
- 23 H. Tanaka and M. Chikazawa, *Mater. Res. Bull.*, 2000, **35**, 75.
- 24 S. Aksel and D. Eder, *J. Mater. Chem.*, 2010, **20**, 9149.
- 25 X. Meng, X-Q. Yang and X. Sun, *Adv. Mater.*, 2012, **24**, 3589.